DISCLAIMER

This report was prepared as an account of work sponsored by an agency of the United States Government. Neither the United States Government nor any agency thereof, nor any of their employees, makes any warranty, express or implied, or assumes any legal liability or responsibility for the accuracy, completeness, or usefulness of any information, apparatus, product, or process disclosed, or represents that its use would not infringe privately owned rights. Reference herein to any specific commercial product, process, or service by trade name, trademark, manufacturer, or otherwise does not necessarily constitute or imply its endorsement, recommendation, or favoring by the United States Government or any agency thereof. The views and opinions of authors expressed herein do not necessarily state or reflect those of the United States Government or any agency thereof. Reference herein to any social initiative (including but not limited to Diversity, Equity, and Inclusion (DEI); Community Benefits Plans (CBP); Justice 40; etc.) is made by the Author independent of any current requirement by the United States Government and does not constitute or imply endorsement, recommendation, or support by the United States Government or any agency thereof.

ORNL/TM-2023/2915
M4LW-23OR04020213

Analysis of Deformation and Fracture Mechanisms in the Harvested Low-Dose Baffle Former Bolt via Advanced Mechanical Tests

M. Gussev
T. Dixon
X. Chen

April 2023

OAK RIDGE National Laboratory

ORNL IS MANAGED BY UT-BATTELLE LLC FOR THE US DEPARTMENT OF ENERGY

ORNL/TM-2023/2915
M4LW-23OR04020213

Nuclear Energy and Fuel Cycle Division
Materials Science and Technology Division

ANALYSIS OF DEFORMATION AND FRACTURE MECHANISMS IN THE HARVESTED LOW-DOSE BAFFLE FORMER BOLT VIA ADVANCED MECHANICAL TESTS

M. Gussev
T. Dixon
X. Chen

April 2023

Prepared under the direction of the
U.S. Department of Energy
Office of Nuclear Energy
Light Water Reactor Sustainability Program
Materials Research Pathway

Prepared by
OAK RIDGE NATIONAL LABORATORY
Oak Ridge, TN 37831
managed by
UT-BATTELLE, LLC
for the
U.S. DEPARTMENT OF ENERGY
under contract DE-AC05-00OR22725

CONTENTS

LIST OF FIGURES iv
LIST OF TABLES iv
ABBREVIATED TERMS v
ACKNOWLEDGMENTS vi
EXECUTIVE SUMMARY vii
1. INTRODUCTION 1
2. MATERIALS 1
2.1 HARVESTED BAFFLE-FORMER BOLTS 1
2.2 SPECIMEN MANUFACTURING 2
3. EXPERIMENTAL ACTIVITIES 3
3.1 MATERIAL COMPOSITION CHECKING 3
3.2 MICROSTRUCTURE BEFORE TESTING 4
3.3 IN SITU MECHANICAL TESTING 5
3.4 NECKING AND MICROFRACTURE EVENTS 7
3.5 MICROSTRUCTURE AND DEFORMATION MECHANISMS AT SMALL STRAINS 9
3.6 DEFORMATION MECHANISMS AT LARGE STRAINS 9
4. SUMMARY AND CONCLUSIONS 10
REFERENCES 11

LIST OF FIGURES

Figure 1. Bolt cutting scheme and IDs for cut objects [1]. 2
Figure 2. Specimens (coupons) used in the current work. 3
Figure 3. EDS maps recorded for the electropolished surface. 4
Figure 4. Typical microstructure for 4416-BS-2 specimen before deformation. 5
Figure 5. A tensile specimen prepared for SEM/EBSD testing. 6
Figure 6. Raw tensile curve recorded during the in situ test. 6
Figure 7. Examples of Kikuchi patterns recorded for 4416-BS-2 BFB specimen. 7
Figure 8. A collage showing low-magnification images recorded at different strain steps. 7
Figure 9. Local fracture event associated with dislocation channeling. 8
Figure 10. Localized fracture and its evolution at different steps. 8
Figure 11. Microstructure at small strains (Step 2, ~1%–1.5% plastic strain) 9
Figure 12. Microstructure at large strains (Step 8, ~20+% plastic strain, exact value to be measured). 10

LIST OF TABLES

Table 1. Fluence and estimated displacement damage distributions for two retrieved BFBs 1
Table 2. Summary of manufactured specimens 3
Table 3. Average compositions of Bolt 4412 compared with material specification for 316 [7] 4

ABBREVIATED TERMS

APT	atom probe tomography
BFB	baffle-former bolt
dpa	displacement per atom
EBSD	electron backscatter diffraction
EDS	energy-dispersive x-ray spectroscopy
GB	grain boundary
HR-EBSD	high–angular resolution electron backscatter diffraction
IMET	Irradiated Materials Examination and Testing Facility
IPF	inverse pole figure
KAM	kernal average misorientation
LAMDA	Low Activation Materials Development and Analysis
ORNL	Oak Ridge National Laboratory
PWR	pressurized water reactor
ROI	region of interest
SEM	scanning electron microscopy

ACKNOWLEDGMENTS

This research was supported by the US Department of Energy, Office of Nuclear Energy, Light Water Reactor Sustainability Program, Materials Research Pathway. Valuable help and support from the staff at ORNL's LAMDA facility (P. Tedder, S. Curlin) and Radiation Control Technician Office are gratefully acknowledged. The authors would like to thank Dr. C. McKinney (ORNL) for reviewing the report and E. Heinrich (ORNL) for helping with document preparation.

EXECUTIVE SUMMARY

This report details the production of ultra-miniature tensile specimens from in-service irradiated baffle-former bolts (BFBs). The report also presents the results of a pilot in situ scanning electron microscopy (SEM)/electron backscatter diffraction (EBSD) test conducted at the Low Activation Materials Development and Analysis facility, located at the US Department of Energy's Oak Ridge National Laboratory. The SEM/EDS results confirmed that the material is AISI 316 steel, not AISI 347. No Nb addition was detected in several analyzed locations. EBSD analysis of the microstructure revealed in-grain misorientation gradients indicative of cold work, likely caused by material processing and BFB manufacturing. No retained ferrite was identified.

During straining, dislocation channel formation was the primary deformation mechanism; twinning was also observed in favorably oriented grains at local strains as small as about 1.5%. No strain-induced phase instability was observed, likely because the Ni and Cr content reached the upper limits for the 316 steel specification.

Multiple microfracture events were observed during the tensile test. Fine strain-induced pores formed at the channel–grain boundary intersection points, and coarser microcracks were associated with nonmetallic inclusions. Data analysis is ongoing, and additional tests are planned in the near future to provide more statistics and details.

1. INTRODUCTION

Baffle-former bolts (BFBs) are important components of pressurized water reactors (PWRs). Nevertheless, they can suffer from radiation-induced degradation while in service in the reactor core during plant operation. Material degradation may reduce the load-carrying capacity and, aggravated by a corrosion environment, eventually lead to cracking. BFB cracking has been a concern for the nuclear industry since the 1980s.

In the United States, degraded BFBs were first observed in 1999. To study the long-term operational performance and reliability of BFBs, the US Department of Energy's (DOE's) Oak Ridge National Laboratory (ORNL), under DOE's Light Water Reactor Sustainability Program's Materials Research Pathway, attempted to harvest two high-fluence BFBs from a commercial Westinghouse two-loop downflow-type PWR. These BFBs had the highest fluence among bolts withdrawn from service in 2011 and did not exhibit any indications of cracking during ultrasonic and visual inspection after removal from service. However, the torque required to remove these bolts from the baffle structure was lower than the original torque specified during installation. The goal was to study the BFB microstructure, mechanical, and corrosion-related properties and estimate the performance of the same components remaining in service.

Two high-fluence BFBs were successfully harvested from a Westinghouse PWR in 2016 and received at the Westinghouse facility for specimen fabrication. The manufactured specimens (thin plates) were delivered to ORNL, where fracture mechanics testing [1,2] and advanced microstructure analysis [3,4] were performed.

This report presents recent results of the advanced mechanical testing performed using in situ scanning electron microscopy (SEM)/electron backscatter diffraction (EBSD) on ultra-miniature specimens manufactured from the BFBs. The results from this study fill knowledge gaps on the in-reactor degradation and deformation mechanisms in this in-service irradiated material used in commercial PWR power plants.

2. MATERIALS

2.1 HARVESTED BAFFLE-FORMER BOLTS

Table 1 provides information on the range of fluences and estimated displacement damage along the length of the two bolts [1,4]. The displacement damage values for the two bolts range from 15 to 41 dpa, assuming a fluence-to–displacements per atom (dpa) conversion value of 6.7×10^{20} n/cm^2, $E > 1$ MeV/dpa [5]. Other important information for the two retrieved bolts not available during this report's preparation includes the irradiation temperature profile and flux.

Table 1. Fluence and estimated displacement damage distributions for two retrieved BFBs

Bolt number	Fluence (10^{22} n/cm^2, E > 1 MeV)/estimated dpa		
	Head	Mid-shank	Mid-thread
4412	2.78/41	2.27/34	1.46/22
4416	1.91/29	1.56/23	1.00/15

The specimen machining scheme and specimens' IDs are shown in Figure 1. For each BFB, four bend-bar specimens and seven thin-slice specimens were machined. The bend-bar specimens were used in the

fracture toughness and fatigue crack growth rate studies [2], whereas the thin-slice specimens were designated for microstructural analyses [3] and advanced mechanical testing like those described in the literature [6].

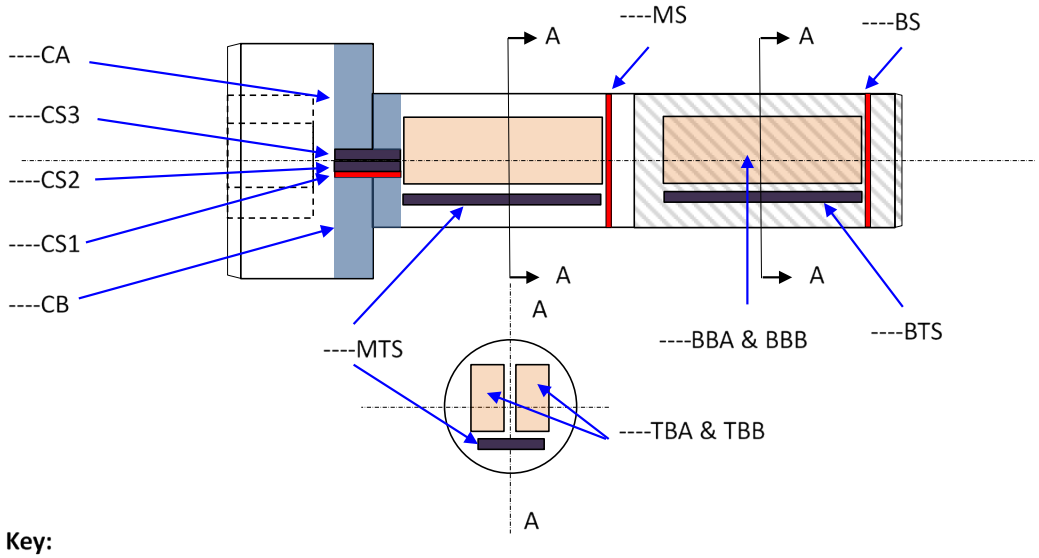

Key:
----: bolt number, **CS**: collar slice, **CA & CB**: remaining collar materials, **MS**: middle slice, **BS**: bottom slice, **MTS**: middle thick slice, **BTS**: bottom thick slice, **TBA & TBB**: top bend bar, **BBA & BBB**: bottom bend bar

Figure 1. Bolt cutting scheme and IDs for cut objects [1]. References [1,2,4] provide more detail.

2.2 SPECIMEN MANUFACTURING

Two specimens of disk-like shape, as shown in Figure 2, were used in the current investigation. The gamma dose rates measured at a 30 cm distance were 120 mrem/h for 4416-MS and 80 mrem/h for 4416-BS. The in-service accumulated damage doses were estimated as 23 dpa for 4416-MS and 15 dpa for 4416-BS. Both specimens had a 0.1 in. (2.54 mm) slice cut away using the low-speed diamond saw at the ORNL Irradiated Materials Examination and Testing facility for microstructural study in 2017/2018. The remaining portion was shipped to the Low Activation Materials Development and Analysis (LAMDA) facility in FY 2022.

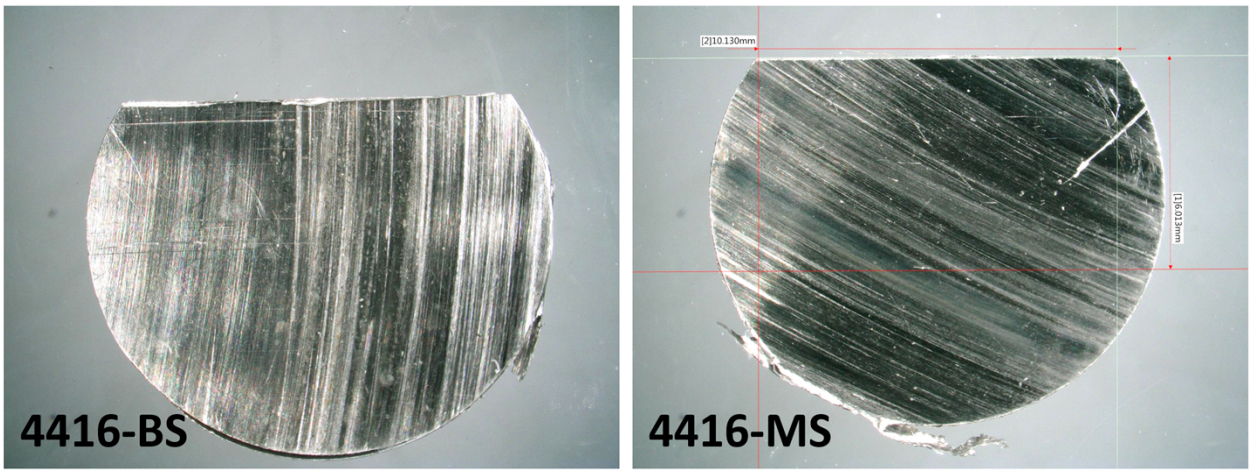

Figure 2. Specimens (coupons) used in the current work. The top portions were cut in 2017/2018 for microstructure analysis.

Four miniature tensile specimens were cut from each coupon using the electric discharge machining system installed in LAMDA's hot area. One specimen per coupon was prepared for SEM/EBSD and micro–digital image correlation (μDIC) testing. The remaining objects are currently stored in LAMDA's storage for future use (Table 2). Additionally, small pieces of the remaining coupon material (one fragment per coupon) were epoxy-mounted and prepared using standard metallography procedures with colloidal silica as the final preparation step. These objects are designated for microstructure analysis, microhardness measurements, and corrosion test trials.

Table 2. Summary of manufactured specimens

Coupons	Specimen	Description
4416-BS	4416-BS-1	Epoxy-mounted small chunk for microstructure analysis
	4416-BS-2	Tensile SS-Teeny specimen for in situ testing
	4416-BS-3	Tensile (kept as is, no preparation).
	4416-BS-4	Tensile
	4416-BS-5	Tensile
4416-MS	4416-MS-1	Epoxy-mounted small chunk for microstructure analysis
	4416-MS-2	Tensile SS-Teeny specimen designated for pilot μDIC test
	4416-MS-3	Tensile (kept as is, no preparation).
	4416-MS-4	Tensile
	4416-MS-5	Tensile

3. EXPERIMENTAL ACTIVITIES

3.1 MATERIAL COMPOSITION CHECKING

Previous reports [4] stated that the bolts are Type 347 austenitic stainless steel. However, later no Nb was observed, and a typical 316 composition was suggested. Energy-dispersive x-ray spectroscopy (EDS) analysis was performed on some of the newly manufactured specimens to confirm the composition further and exclude any possibility of local composition variations. The results and previously obtained atom

probe tomography (APT) data [7] are shown in Table 3. The APT results agree well with the recent EDS results for different coupon/specimen locations, confirming 316 composition. No Nb was observed.

Table 3. Average compositions of Bolt 4412 compared with material specification for 316 [7]

Element	EDS in the current work (average results for several scans) (wt %)	APT reconstructions [7] (wt %)	UNS S31600 specification (wt %)
Fe	Bal.	Bal.	Bal.
Ni	11.6	12.22	10.00–14.00
Cr	17.7	18.11	16.00–18.00
Mn	1.6	1.60	2.00 max
Mo	2.1	2.04	2.00–3.00
Si	0.5	0.63	1.00 max
C	n/d	0.043	0.08 max
P	n/d	0.013	0.040 max
S	n/d	N/A	0.030 max
Cu	0.4	0.29	0.75 max

Note: Averages were calculated from 12 APT reconstructions (4 from each section of the bolt).

Spatial element mapping, Figure 3, shows the presence of Mn-, Si-, and O-rich clusters, likely inclusions of metallurgical origin (#1, #2 in Figure 3). Few scattered carbon-rich objects (small carbides, #3 in Figure 3) present as well. Multiple Mo- and Mn-rich objects of micron-scale were observed, being likely intermetallic compounds (#4 in Figure 3). The overall density, size, and morphology of inclusions is typical for commercial nuclear-grade 316 steel.

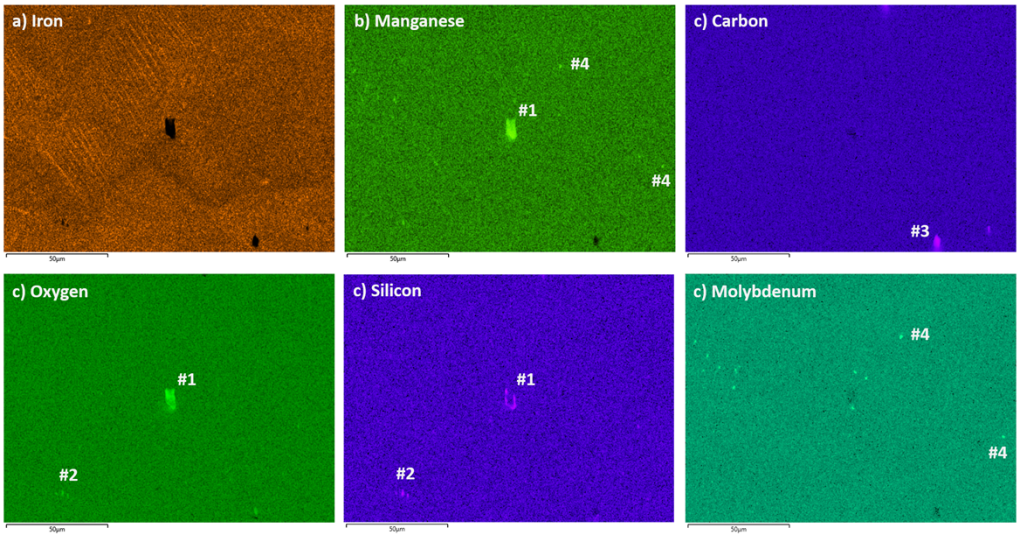

Figure 3. EDS maps recorded for the electropolished surface.

3.2 MICROSTRUCTURE BEFORE TESTING

Figure 4 shows the typical microstructure for the BFB material from 4416-BS-2 (i.e., for the back slice). Equi-axial austenite grains with some in-grain misorientation gradients are visible. Color gradients in the

inverse pole figire (IPF) maps are smooth, without sharp variations in colors or line-like features (dislocation channels) typical for postirradiation deformation. The misorientation variations may be caused by deformation during material processing and BFB manufacturing. Some coarse inclusions of metallurgical origin are present in the structure, but their volume fraction is low enough and not of concern. Interestingly, no retained ferrite was observed in the microstructure.

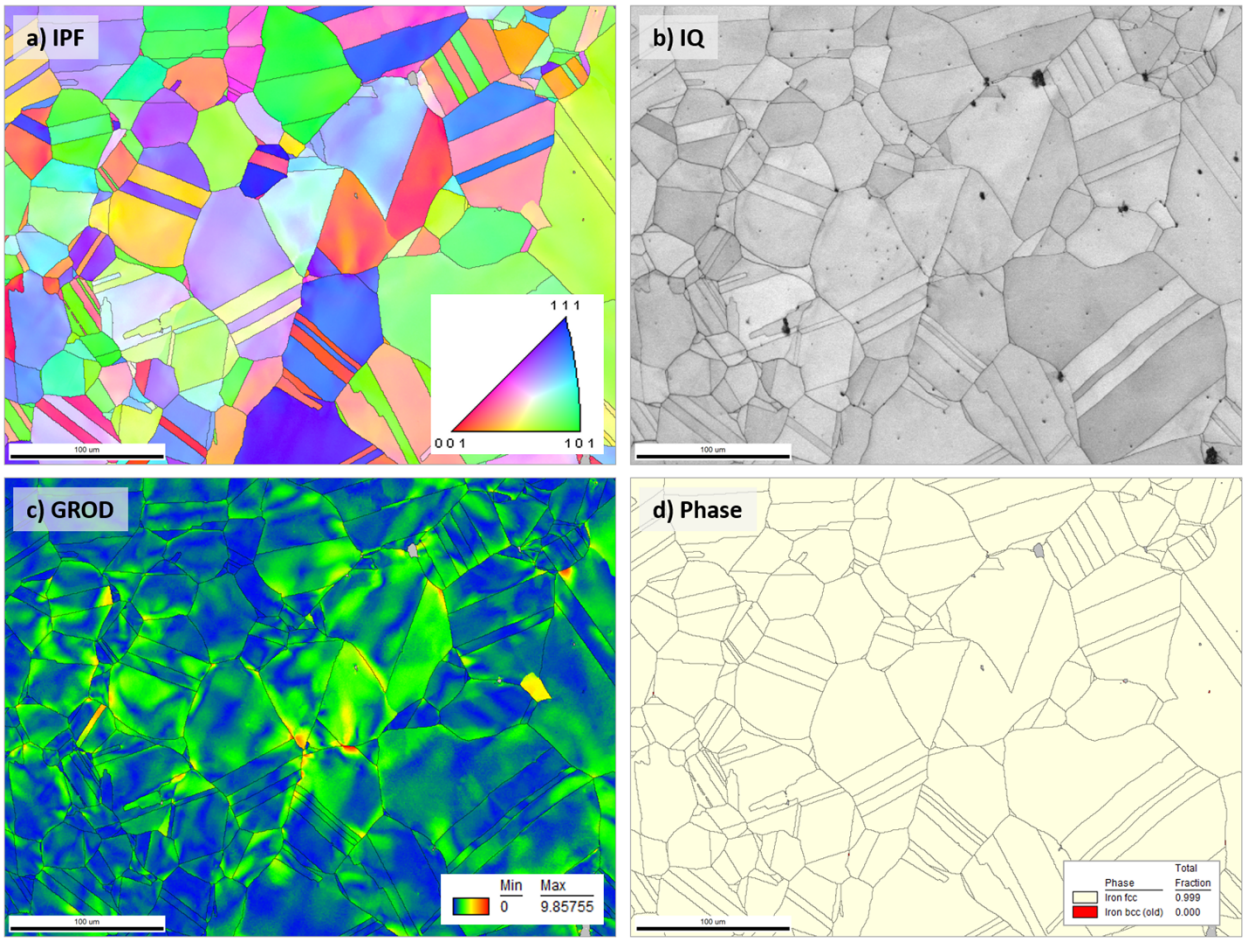

Figure 4. Typical microstructure for 4416-BS-2 specimen before deformation. (a) EBSD inverse pole figure [IPF], (b) Image quality [IQ], (c) grain reference orientation deviation [GROD], and (d) phase maps. This region of interest (ROI) was tracked and rescanned during the in situ test. Note fully austenitic structure with no retained ferrite. IPF map is colored in the tensile (horizontal) direction; the IPF color key is the same for all IPF maps in the document.

3.3 IN SITU MECHANICAL TESTING

Figure 5 shows the in-house manufactured tensile specimen prepared for SEM/EBSD in situ testing. The specimen has a clean surface with few scattered non-metallic inclusions smaller than about 5–7 μm in size. No stringers, large rough inclusions, corrosion cracks, or coarse ferrite grains were observed.

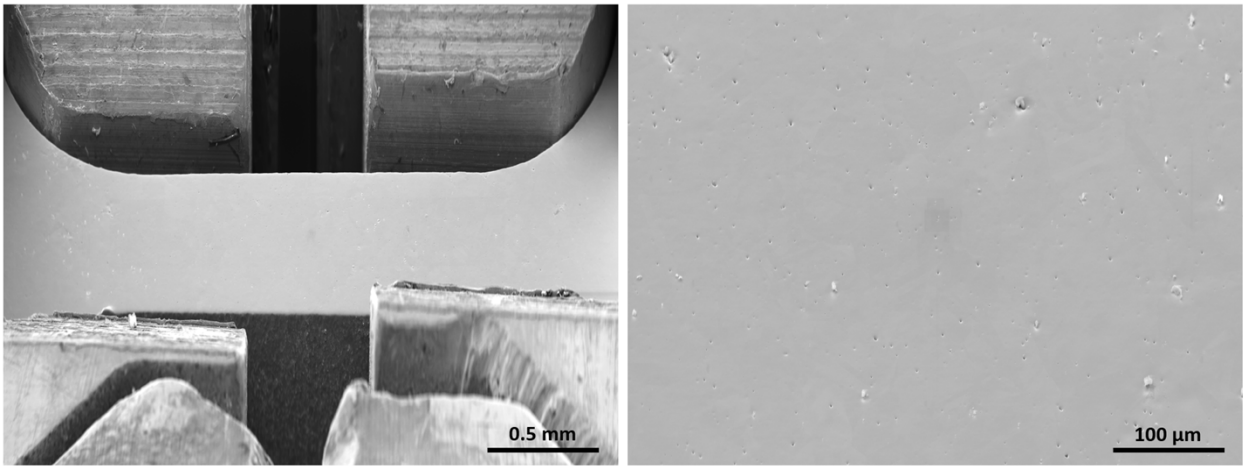

Figure 5. A tensile specimen prepared for SEM/EBSD testing. (left) in the grips before the test and (right) electro-polished surface view. The SEM images were recorded at 70° tilt with dynamic focus correction.The experiment started with selecting and pre-mapping regions of interest (ROIs) (Figure 4). After that, nine strain steps were performed. Figure 6 shows the tensile curve. EBSD scans and SEM images were recorded as necessary to document the strain-induced changes.

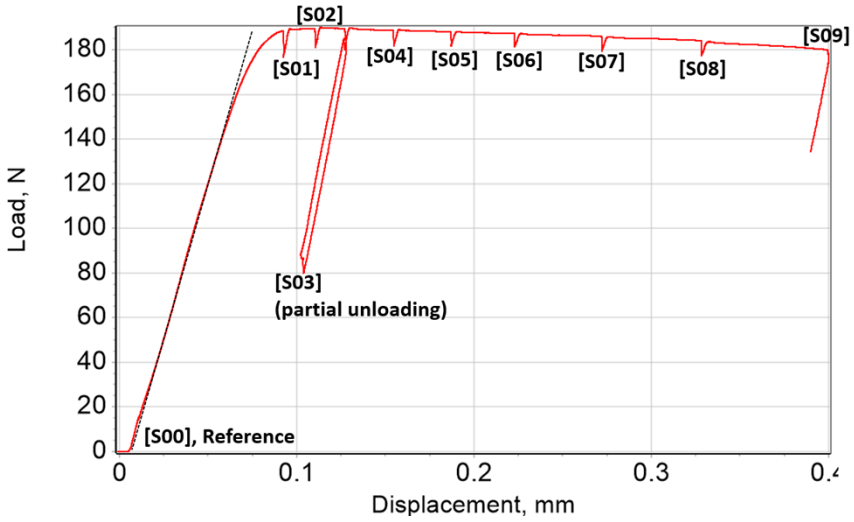

Figure 6. Raw tensile curve recorded during the in situ test.

High–angular resolution EBSD (HR-EBSD [8]) scanning was performed before testing and at steps 1 and 2. Unfortunately, strain-induced morphology does not allow HR-EBSD analysis at large strains without specimen polishing. HR-EBSD requires recording and storing high-quality Kikuchi patterns, as shown in Figure 7, and allows for calculating in-grain elastic strains/stresses and geometrically necessary dislocation densities.

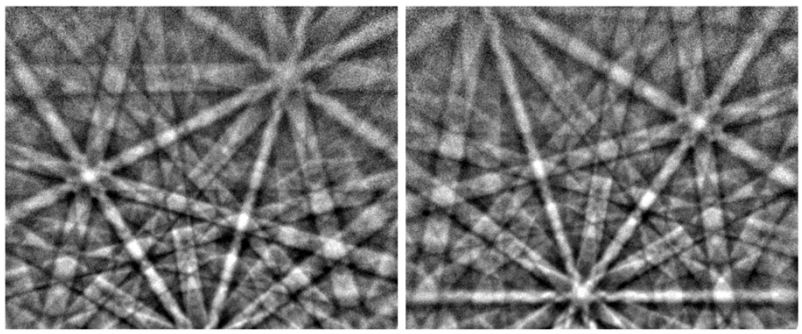

Figure 7. Examples of Kikuchi patterns recorded for 4416-BS-2 BFB specimen.

3.4 NECKING AND MICROFRACTURE EVENTS

Figure 8 shows the specimen's gauge and strain-induced changes along the gauge. Diffuse neck forms immediately after the yield stress is reached. The neck occupied ~2/3 of the gauge (Step 2, [S02]). At step 4, localized necking started to develop, and strain-induced localized micro-fracture events became evident.

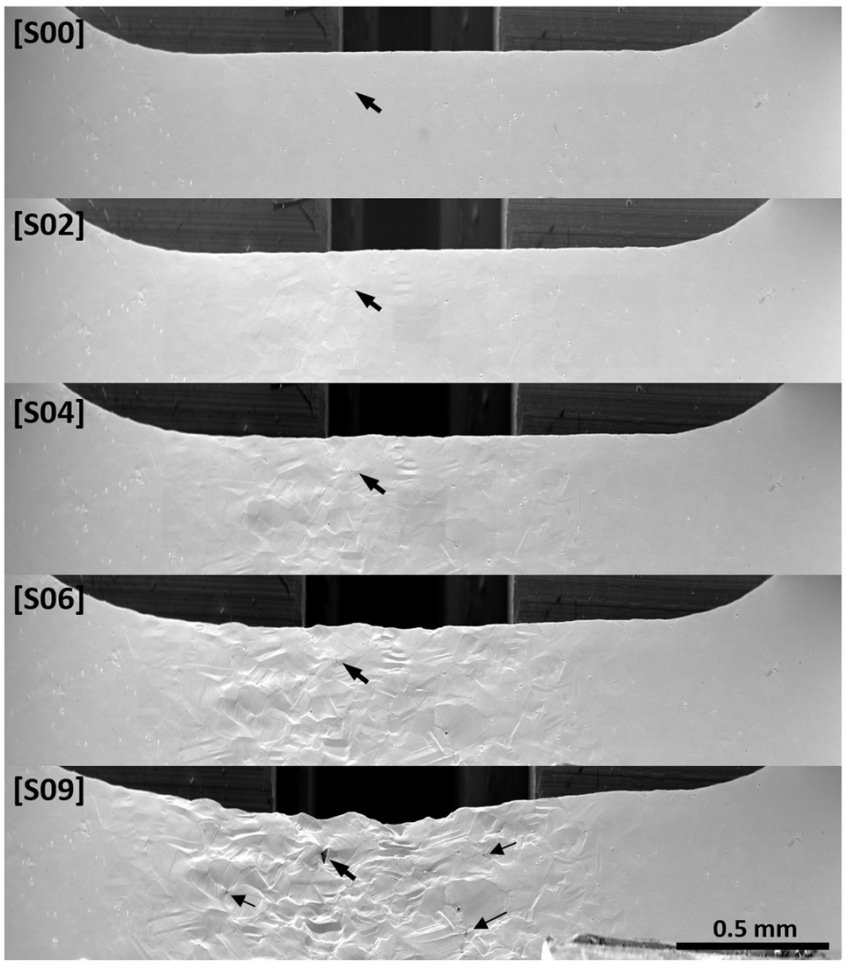

Figure 8. A collage showing low-magnification images recorded at different strain steps. Bold arrows point to a notable fracture event and track it back to the reference (step 0 [S00]) image. Fine arrows point to other micro-fracture locations. The steps are shown in Figure 6.

Several strain-induced pores appeared at the channel–grain boundary (GB) intersection (Figure 9). Localized deformation at the channel–GB point formed a depression at the surface first (Figure 9a). With further strain increase, many such depressions evolved into pores.

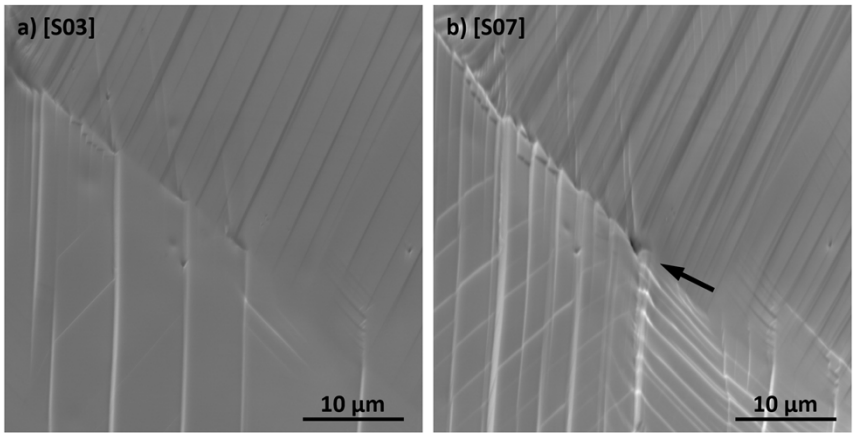

Figure 9. Local fracture event associated with dislocation channeling. The black arrow points to micropore formation.

More coarse cracks (10–20 µm and more) were associated with nonmetallic inclusions and their cracking during straining, as shown in Figure 10a. Such inclusion-associated cracks could grow quickly via ductile tearing, as illustrated in Figure 10b. Crack development was accompanied by pronounced cross-slipping and activation of secondary slip systems in the crack-surrounding grains. After the largest visible crack reached about 50–60 µm in length, the experiment was stopped: this or another defect could have grown quickly and caused sudden fracture (fracturing irradiated specimens inside SEM instruments is not allowed by current safety rules). The number of observed pores and microcracks was much higher than all irradiated specimens tested previously (304L and 316L steels irradiated in BOR-60 fast reactor, 304L steel irradiated to 4.4. dpa in boiling water reactor).

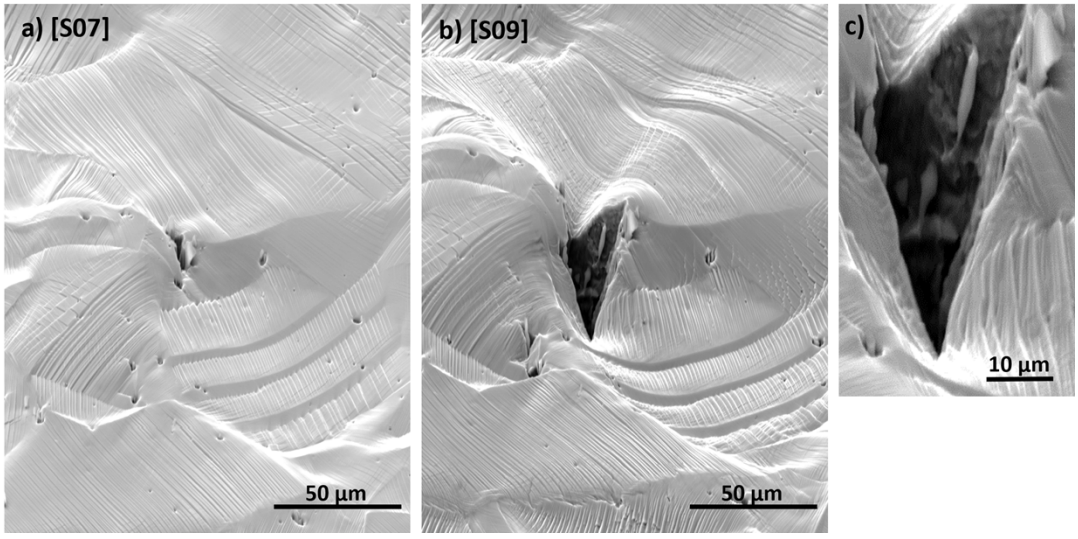

Figure 10. Localized fracture and its evolution at different steps. (a) step 7 (S07) and (b) step 9 (S09). An inset in (c) shows a magnified view of the crack interior; note the elongated or "spindle-like" shapes of the inclusions in the crack interior.

3.5 MICROSTRUCTURE AND DEFORMATION MECHANISMS AT SMALL STRAINS

Dislocation channeling was a dominating mechanism at small strains. Multiple channels are easy to see in the IQ map, Figure 11b. Most channels (e.g., those in grain G_1) show weak, if any, variations in the kernel average misorientation (KAM) map (Figure 11c), suggesting relatively low in-channel dislocation densities. However, some channels appeared in the KAM map (grain G_4 and the channel marked with an arrow). This channel extended through the grain, and its right portion appears to have high dislocation density.

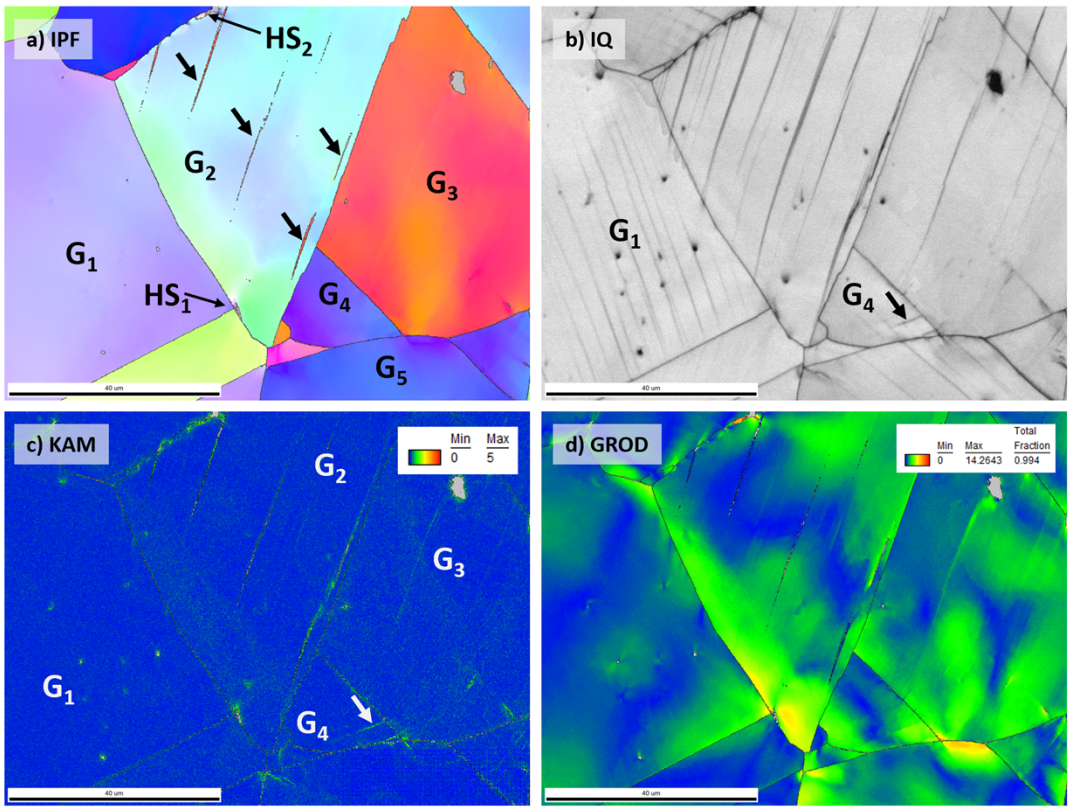

Figure 11. Microstructure at small strains (Step 2, ~1%–1.5% plastic strain). Dislocation channels, along with multiple fine twins within the channels in one of the grains, are visible in the IQ map.

A specific "hot spot" (HS_1 in IPF map, Figure 11a) became evident. This area with high local misorientation (and thus high local dislocation density) formed at the triple junction point. Another object, HS_2, appeared as an area surrounded by a strain-induced boundary. The hot spots likely form because of highly localized deformation. Whereas dislocation slipping and channeling should be key deformation modes inside the spots, the formed channels/slip lines are fine and do not propagate far from the start point. Such spots with high local dislocation density may stimulate localized corrosion processes.

Strain-induced twinning became evident instead of small strains. Fine needle-like twins formed inside defect-free channels (G_2 in Figure 11). In some cases, twin formation led to elevated local KAM values.

3.6 DEFORMATION MECHANISMS AT LARGE STRAINS

Figure 12 shows microstructure processes inside the growing localized neck at large local strains. Surface morphology becomes well developed at this strain level, leading to "bent" slip line traces in the EBSD

maps. This minor methodical issue complicates the slip system analysis but does not affect deformation mechanism identification.

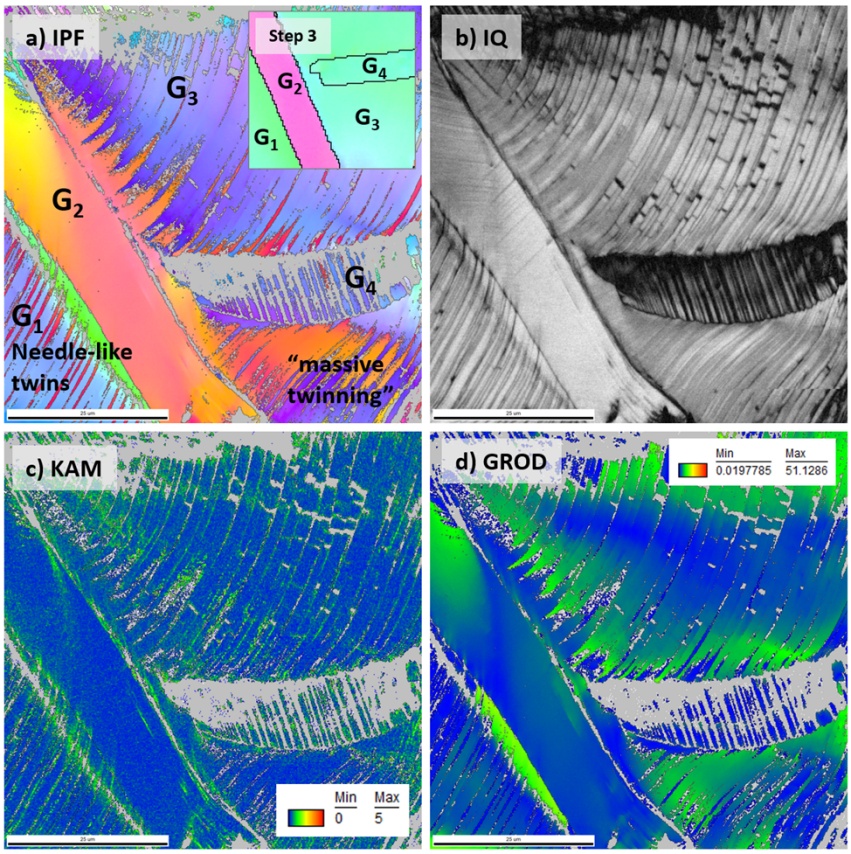

Figure 12. Microstructure at large strains (Step 8, ~20+% plastic strain, exact value to be measured). Of immediate interest is the massive twinning observed in some grains. The dark gray color shows non-indexed areas. An inset in the IPF map shows the grain structure at small strains (Step 3).

Dislocation channeling remained an important deformation mode; however, strain-induced twinning also became an important mechanism. Sharp, needle-like twins populated most of the grains. Whereas some grains (e.g., G_1) showed common twin morphology (needles, fine plates), a specific "massive" twinning became evident as well (G_3). In this grain, strain-induced twins had a needle-like morphology at small strains but later started to widen near the twin–GB intersection, forming triangle-like objects and massive, 10 μm wide twins. As expected, such a mechanism may severely disturb the protective oxide layer, stimulating local corrosion.

Massive twinning was common in this BFB material (multiple areas were observed), compared with only one weak event in all previously tested specimens. Further data analysis is in progress.

4. SUMMARY AND CONCLUSIONS

In conclusion, this report presents the results of a pilot in situ SEM/EBSD test conducted at ORNL's LAMDA facility using tensile specimens made from in-service irradiated BFBs. The SEM/EDS analysis confirmed that the material is AISI 316 steel and revealed in-grain misorientation gradients indicative of cold work. No retained ferrite was identified, and no strain-induced phase instability was observed, likely because the Ni and Cr content reach the upper limits for the 316 steel specification.

During straining, dislocation channel formation was found to be the primary deformation mechanism. Twinning was also observed in favorably oriented grains at local strains as small as about 1.5%. Furthermore, multiple microfracture events were observed during the tensile test: fine strain-induced pores formed at the channel–grain boundary intersection points, and coarser microcracks associated with nonmetallic inclusions were observed.

Data analysis is ongoing, and additional tests are planned to provide more statistics and details. Nonetheless, the initial results demonstrate the potential of in situ SEM/EBSD testing for characterizing irradiated materials and the importance of understanding the deformation mechanisms and fracture behavior of these materials.

REFERENCES

[1] K.J. Leonard, M.A. Sokolov, M.N. Gussev, Post-Service Examination of PWR Baffle Bolts, Part I. Examination and Test Plan, Oak Ridge National Laboratory Report, ORNL/LTR-2015/193, 2015.

[2] X.F. Chen, M.A. Sokolov, Fracture Toughness and Fatigue Crack Growth Rate Testing of Baffle-Former Bolts Harvested from a Westinghouse Two-Loop Downflow Type PWR, Oak Ridge National Lab.(ORNL), Oak Ridge, TN (United States), 2021.

[3] T. Lach, X. Chen, T.M. Rosseel, Microstructural Characterization of the Second High Fluence Baffle-Former Bolt Retrieved from a Westinghouse Two-loop Downflow Type PWR, Oak Ridge National Lab.(ORNL), Oak Ridge, TN (United States), 2022.

[4] X.F. Chen, T. Chen, C.M. Parish, T. Graening, M.A. Sokolov, K.J. Leonard, Post-Irradiation Examination of High Fluence Baffle-Former Bolts Retrieved from a Westinghouse Two-Loop Downflow Type PWR, Oak Ridge National Lab.(ORNL), Oak Ridge, TN (United States), 2019.

[5] O.K. Chopra, A.S. Rao, Degradation of LWR Core Internal Materials due to Neutron Irradiation, 2010.

[6] M.N. Gussev, K.J. Leonard, In situ SEM-EBSD analysis of plastic deformation mechanisms in neutron-irradiated austenitic steel, Journal of Nuclear Materials. 517 (2019) 45–56.

[7] T. Lach, X. Chen, T. Rosseel, Microstructural Characterization of the Second High Fluence Baffle-Former Bolt Retrieved from a Westinghouse Two-loop Downflow Type PWR, 2022.

[8] A.J. Wilkinson, G. Meaden, D.J. Dingley, High-resolution elastic strain measurement from electron backscatter diffraction patterns: new levels of sensitivity, Ultramicroscopy. 106 (2006) 307–313.